Bragg Scatter Detection by the WSR-88D. Part I: Algorithm Development

LINDSEY M. RICHARDSON,[a,b] JEFFREY G. CUNNINGHAM,[c] W. DAVID ZITTEL,[a] ROBERT R. LEE,[a] RICHARD L. ICE,[a,c] VALERY M. MELNIKOV,[d,e] NICOLE P. HOBAN,[f,g] AND JOSHUA G. GEBAUER[f,h]

[a] *Radar Operations Center, National Weather Service, Norman, Oklahoma*
[b] *Centuria Corporation, Norman, Oklahoma*
[c] *557th Weather Wing, Offutt Air Force Base, Nebraska*
[d] *Cooperative Institute for Mesoscale Meteorological Studies, University of Oklahoma, Norman, Oklahoma*
[e] *National Severe Storms Laboratory, Norman, Oklahoma*
[f] *Research Experiences for Undergraduates, National Weather Center, Norman, Oklahoma*
[g] *North Carolina State University, Raleigh, North Carolina*
[h] *University of Oklahoma, Norman, Oklahoma*

(Manuscript received 25 January 2016, in final form 6 December 2016)

ABSTRACT

Studies have shown that echo returns from clear-air Bragg scatter (CABS) can be used to detect the height of the convective boundary layer and to assess the systematic differential reflectivity (Z_{DR}) bias for a radar site. However, these studies did not use data from operational Weather Surveillance Radar-1988 Doppler (WSR-88D) or data from a large variety of sites. A new algorithm to automatically detect CABS from any operational WSR-88D with dual-polarization capability while excluding contamination from precipitation, biota, and ground clutter is presented here. Visual confirmation and tests related to the sounding parameters' relative humidity slope, refractivity gradient, and gradient Richardson number are used to assess the algorithm. Results show that automated detection of CABS in operational WSR-88D data gives useful Z_{DR} bias information while omitting the majority of contaminated cases. Such an algorithm holds potential for radar calibration efforts and Bragg scatter studies in general.

1. Introduction

a. Bragg scatter background

Since the completion of the dual-polarization upgrade to the Weather Surveillance Radar-1988 Doppler (WSR-88D), users have been able to make more detailed assessments of the atmosphere. One phenomenon of interest is clear-air Bragg scatter (CABS). Specifically, it has been shown that CABS can be used to assist with radar calibration and detection of the height of the convective boundary layer (Melnikov et al. 2011, 2013a; Cunningham et al. 2013; Zittel et al. 2014). This paper describes the development and testing of an automated algorithm for detecting CABS on operational WSR-88Ds.

Bragg scatter is caused by turbulent inhomogeneities with sizes around one-half of a transmitted radar wavelength (e.g., Cowley 1995; Hardy and Katz 1969; Knight and Miller 1993; Doviak and Zrnić 2006, chapter 11). Bragg scatter has been observed as a layer in clear air and developing clouds, and it is mostly associated with refractivity gradients (Atlas 1959; Ottersten 1969). Studies have found that refractivity gradients are related to gradients of moisture in dynamically unstable regions (Ottersten 1969; Hardy and Katz 1969; Hardy and Ottersten 1969). In maritime environments, moisture proved to be a more important factor than temperature, and the primary generation mechanisms consisted of turbulent mixing and detrainment/entrainment of cloudy air (Knight and Miller 1993, 1998; Cohn 1994; Gage et al. 1999; Davison et al. 2013a,b).

Melnikov et al. (2011, 2013a) used Bragg scatter to detect the height of the turbulent convective boundary

Corresponding author e-mail: Lindsey M. Richardson, lindsey.m.richardson@noaa.gov

DOI: 10.1175/JTECH-D-16-0030.1

layer in a continental environment. Information about the dual-polarization field characteristics allowed them to easily distinguish biota and precipitation from CABS. Their results showed that Bragg scatter corresponds with strong vertical gradients of humidity. Both Davison et al. and Melnikov et al. suggest that soundings could be used to indicate layers conducive to producing Bragg scattering (discussed in section 3b).

b. Practical application of Bragg scatter

The turbulent eddies associated with CABS are randomly oriented and thus have an intrinsic differential reflectivity (Z_{DR}) near 0 dB on an unbiased system (Melnikov et al. 2011, 2013a). External targets with known intrinsic Z_{DR} values, such as CABS, can be used to independently verify the systematic bias of Z_{DR} (Z_{DR} bias) of a radar site. Thus, CABS without contamination can be a potential estimator of the Z_{DR} bias. The Z_{DR} bias within the WSR-88D can be introduced via an engineering-derived internal parameter known as ZDR_{Offset}. This ZDR_{Offset} is applied automatically to the measured Z_{DR} field (Cunningham et al. 2013; Melnikov et al. 2013b). If the ZDR_{Offset} fails to capture correctly some aspect of hardware bias, the result is a bias in Z_{DR}. Thus, an error in ZDR_{Offset} translates to a Z_{DR} bias. CABS returns with Z_{DR} estimates not near 0 dB reflect a bias in the radar.

Results from initial development and testing of an automated algorithm to collect Z_{DR} bias estimates from CABS in radar data are presented here. Datasets in this study span from October 2013 through September 2014 from over 130 WSR-88D radar sites across the United States.[1] Archived operational Level II[2] data were processed offline in a MATLAB environment from sites across the contiguous United States (CONUS) and outside-CONUS (OCONUS) sites, such as Alaska, Hawaii, and Puerto Rico. Section 2 describes an algorithm to detect CABS with the operational dual-polarization WSR-88Ds with a focus on Z_{DR} calibration aspects. Section 3 covers results from visual confirmation and compares the algorithm output to sounding tests followed by a summary and a discussion in section 4.

2. Bragg scatter detection algorithm

a. Algorithm overview

Preliminary visual confirmation and knowledge of the dual-polarization characteristics of Bragg scatter (e.g., Melnikov et al. 2011) were used to formulate a specific setup for capturing CABS data. Reflectivity (Z), velocity (V), spectrum width (W), correlation coefficient (ρ_{HV} or CC), and signal-to-noise ratio (SNR) are used to identify a potential CABS layer and filter out contaminants (described further in sections 2d and 2e). These fields are collectively referred to as base data.[3]

There are six main steps for identifying a potential CABS layer and estimating the Z_{DR} bias from the returns on a WSR-88D:

1) Find radar data within certain spatial limits over a certain time domain.
2) Create a Z histogram of data within the spatial and temporal limits.
3) Create a separate Z_{DR} histogram of range gates that pass base data filters using the same spatial limits applied over the specified time domain.
4) Use statistical filters to assess Z_{DR} histogram data for statistical validity and potential contamination from non-Bragg sources.
5) Use a precipitation filter to further reduce the likelihood of contamination.
6) Calculate the mode of the Z_{DR} histogram if it passes all previous filters.

For this study, specific range limits, elevation angles, and volume coverage patterns (VCPs) mitigate clutter and some precipitation contamination (described further in section 2b). Values of Z from passing range gates within the spatial limits are collected into a histogram over a certain time window for further statistical testing. We used the 1700–1900 UTC time window for our initial testing, though CABS is not limited to this time domain (section 2c). A Z_{DR} histogram is created using the same VCP, spatial, and temporal limits, but only range gates that pass the base data filters (section 2d) are included in the distribution. A test for the sample size and spread of the Z_{DR} histogram is used to check the statistical validity of the distribution and potential contamination (section 2e). Next, the separate Z histogram for precipitation contamination (section 2f) is checked. Finally, once these filters are passed, the mode from the Z_{DR} histogram is calculated as an assessment of Z_{DR} bias from CABS-like returns.

b. Volume coverage pattern and range limits

CABS layers are expected to lie at the top of a boundary layer (convective or marine) a majority of the

[1] Radar data were not always available every day for each radar site due to radar downtime/data feed errors.

[2] See Crum et al. (1993) for the distinction between the various levels of radar data available.

[3] The differential phase (Φ_{DP}) is also a dual-polarization base variable, but the Φ_{DP} characteristics of CABS is similar to the characteristics of light precipitation. Thus, we opted to not use Φ_{DP} for this study.

time. Several studies show that the convective boundary layer is generally no higher than 3 km (~10 000 ft) above ground level (AGL; Kaimal et al. 1982; vanZanten et al. 1999; Stensrud 2007, chapter 5; Heinselman et al. 2009). To cover the heights where CABS has been observed, a range limit of $10 \leq R \leq 80$ km was selected. Given typical WSR-88D scanning angles, CABS is less likely to be detected beyond 80 km (~43 n mi) and still fill the radar beam[4] in operational WSR-88D volume scans. Additionally, data within 10 km (~5 n mi) are susceptible to ground clutter and sidelobe contamination and were excluded. While most previous studies have been in very specific climate regimes, the range of observable CABS from WSR-88D data was unknown across many regimes. A preliminary case from Lubbock, Texas (KLBB), showed CABS at nearly 80 km (at the 2.4° elevation angle), which helped determine the maximum range on which to test in this initial algorithm (not shown). Superrefraction, where the radar beam bends toward the ground, can also allow the detection of CABS at farther ranges.

Operational WSR-88Ds use predefined VCPs that vary in the number of elevation angles they scan, how fast they scan, and how many pulses are sampled. Only VCPs 32 and 21[5] were considered in this study in order to reduce the overall chance for precipitation contamination. VCP 32 is considered a clear-air VCP (see Crum et al. 1993), but some radar sites rarely use this clear-air VCP. We have included VCP 21 data in this study to capture CABS from more sites across the fleet. Only elevation angles between 2.4° and 4.5° are considered (only three elevations angles in each VCP); angles above 4.5° exceed 3-km AGL for a majority of the 10–80-km range. Starting at 2.4° avoids most ground clutter contamination, and we facilitate locating a layer by examining multiple elevation angles.

An operational cut of WSR-88D data consists of a single 360° scan at a specific elevation angle. For simplicity, we avoid using split-cut (multiple scans at the same elevation angle) data because the base data would be collected across two scans that are not coincident in time. We avoid using VCP 31 because it includes a split-cut at 2.5°. Additionally, many sites use VCP 31 exclusively in light precipitation (especially snow) cases.

c. Time considerations

For initial widespread testing, a time window of 1700–1900 UTC was chosen to analyze the October 2013–September 2014 data. This time frame corresponds well with heating and convective boundary layer mixing (in the central plains of the United States). However, it could be too early for some western areas and too late for some eastern areas. CABS is not guaranteed to have development preference from 1700 to 1900 UTC at any given site nor is CABS limited to a 2-h window. On a daily basis, all volume scans from allowed VCPs and elevation angles within the time window from a single WSR-88D represent a data case in this study.

d. Base data filters

Melnikov et al. (2011) discuss the main dual-polarization characteristics of typical CABS layers. Figure 1a shows an example of how these layers generally appear as rings on WSR-88D scans.[6] Note the low Z returns, which are usually less than 0 dBZ. More notable in the Z_{DR} field, CABS is characterized by low Z_{DR} (compared to the clutter field close to the radar with higher Z_{DR}). Thresholds related to the base data are used as a filter to retain range gates associated with CABS. These base data filters are applied to each range gate for each cut [Eq. (1)], where

$$Z < 10 \text{ dB}Z, \tag{1a}$$

$$\text{SNR} < 15 \text{ dB}, \tag{1b}$$

$$\rho_{HV} \geq 0.98, \tag{1c}$$

$$|V| > 2 \text{ m s}^{-1}, \tag{1d}$$

$$W > 0 \text{ m s}^{-1}. \tag{1e}$$

Values of Z_{DR} are retained only from range gates that pass these base data thresholds. Here Z_{DR} itself is not used as a filter because the goal is to assess Z_{DR} bias.

CABS is a generally weak echo return at S band, thus the Eqs. (1a) and (1b) requirements. While returns are usually 0 dBZ or less, we allow up to 10 dBZ in our algorithm to avoid eliminating potential cases in the initial development. It has been previously shown that dual-polarization signals at low SNR can be biased (e.g., Melnikov and Zrnić 2007), but the implementation

[4] The beamwidth of the WSR-88D to the half-power point is ~0.95°.

[5] Similar VCPs 34 and 24 were allowed but only available at KLGX (Langley Hill, Washington). KLGX now uses VCP 32 and 21 with one extra scan. Please refer to the Radar Operation Center's interface control document (ICD) for radar acquisition (RDA)/radar product generator (RPG) for more details about each VCP (http://www.roc.noaa.gov/WSR88D/BuildInfo/Files.aspx).

[6] The WSR-88D has a minimum detectable signal of around −10 dBZ (at 50 km, in short pulse, and 2-dB SNR in VCP 21 and 1-dB SNR in VCP 32) and a typical sample volume radar range gate size of 1 km × 1 km × ¼ km.

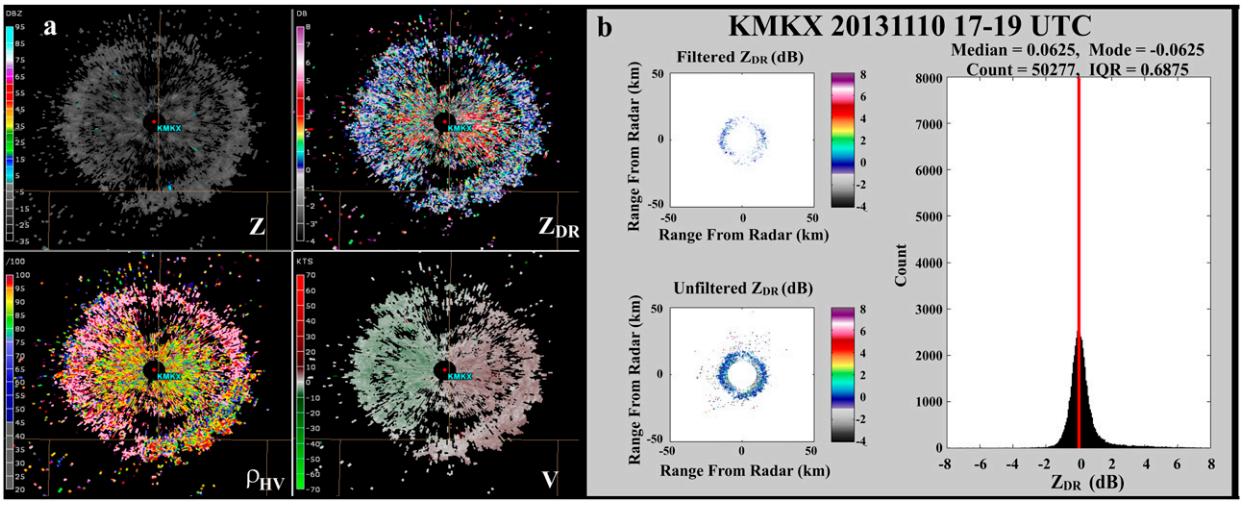

FIG. 1. Bragg example from Milwaukee, WI (KMKX), on 10 Nov 2013. (a) The WSR-88D plan position indicator (PPI) images show (upper left) Z, (upper right) Z_{DR}, (lower left) ρ_{HV}, and (lower right) velocity from the 3.5° elevation angle at 1852 UTC. Maximum range in the radar image shown is ~22 km. (b) The Z_{DR} histogram shows the (top left) range gates that pass the base data filters [Eq. (1)], (bottom left) all of the range gates, and (right) the histogram of points that pass the base data filters. Zero decibel is marked by the red line in the histogram. All PPI images use default National Weather Service color scales, which could be modified for more detailed studies of the CABS characteristics in future work.

of the radial-by-radial noise technique on the WSR-88D mitigates this concern (Ivić et al. 2013, 2014; Ivić 2014). Returns are typically uniform in CABS, hence the focus on higher correlation coefficient values [Eq. (1c)]. Equations (1d) and (1e) help avoid clutter, which is often characterized by near 0 m s^{-1} V and W. All of the base data filters use the precision units specified in the system specifications of the WSR-88D (WSR-88D ROC 2008). For example, because the precision of W is 0.5 m s^{-1}, any value between 0 and 0.5 m s^{-1} is set to 0 m s^{-1} on the WSR-88D.

e. *Statistical filters*

The Z_{DR} values that pass the base data filters are stored in the appropriate class interval in a histogram that is accumulated over the 2-h window and are saved for further processing. The class interval of 0.0625 dB matches the precision of WSR-88D Level II Z_{DR} data. We do not require any minimum count of range gates by elevation or volume scan but instead use all of the range gates collected over a 2-h window. An example of a histogram of range gates that pass the base data filters is shown in Fig. 1b. The shape is relatively Gaussian with a slightly longer tail of positive Z_{DR} values. The slightly longer tail is expected due to the likely biota returns closer to the radar. Each 2-h window was isolated per radar per day; neither multiple estimates per day nor 2-h windows spanning multiple days were considered in this study.

Statistical filters were applied to the 2-h cumulative histogram. A minimum total range gate count requirement of 10 000 range gates helps ensure a statistically reliable sample size. CABS histograms with little to no contamination are generally Gaussian with a mode centered on 0.0 dB from an unbiased radar. Cases with more contamination, especially from biota and ground clutter, produce wider histograms. The interquartile range (IQR), defined as the 75th percentile minus the 25th percentile, assesses the overall spread of the histogram (Wilks 2006) and can distinguish cases with excessive contamination. A preliminary case analysis using 20 sites from May to August 2013 during the 1700–1900 UTC time window revealed that most CABS cases have an IQR less than 0.9 dB, while contaminated cases have higher IQR and lower kurtosis. Thus, the authors require an IQR less than 0.9 dB on the Z_{DR} histogram for the case to be considered valid CABS for a given day. The IQR was found to be more useful than a skewness test for filtering out contamination (also seen in Hoban et al. 2014). Biota/clutter can produce either a positive or a negative skew, or no net skew if both positive and negative contributions are in the same distribution, but these are mostly filtered out by the ρ_{HV} threshold in the base data filters. Precipitation generally broadens the histogram (without introducing skewness) and is removed via the IQR threshold. However, light precipitation may still pass the IQR threshold.

f. *Precipitation filter*

An additional precipitation filter is necessary because light precipitation mimics many CABS radar characteristics. A subset of select days in October 2013–March 2014 from 98 sites (919 cases total) were analyzed to

discover the statistical differences between precipitation-contaminated cases and CABS cases. Using a cool-season time frame reduced the chance for biota contamination in a majority of sites across the United States while increasing the likelihood of capturing precipitation cases (particularly light snow) for testing the filter design. To facilitate the evaluation of a precipitation filter, radar data experts visually classified radar returns within the specified spatial and temporal limits (1700–1900 UTC) into four main categories:

1) CABS—CABS with no visible contamination
2) None—Clear air, clutter, or biota without CABS, or CABS too close to radar
3) Mixed—CABS and some visible contamination
4) Precip—Precipitation only (little or no CABS overall)

Each case was categorized by visually analyzing Level II data across the 2-h window to look for characteristics similar to those shown in Fig. 1. Ranges and elevation angles matching the algorithm thresholds were given priority for investigation. All of the cases were from the VCPs of interest, but the base data and statistical filters were not applied. During the visual categorization, the potential for contamination was given priority over CABS characteristics, such as uniformity of returns or thickness of the layer.

Cases were classified as CABS when CABS and no visible contamination were noted during the 2-h time frame. Because characteristics of small cloud particles are similar to CABS, some contamination could have been inadvertently included in this category. However, any contaminants with intrinsic Z_{DR} values near 0 dB do not harm bias estimation results. Cases without any visible CABS that had only biota/clutter returns were classified as None. Cases with a small ring of Bragg scatter less than 10 km from the radar (not within our range limits) were also classified as None.

Mixed cases include CABS and contamination (precipitation, clutter, and/or biota) having been identified somewhere within the defined range and elevation angle limits. Contamination may be collocated with the CABS or in different range gates anywhere within the spatial and temporal limits. Cases with even one elevation angle from one volume scan with visible contamination were classified as Mixed. For example, in the event of precipitation moving into (out of) the area during the time window, cases fall into the Mixed category if CABS was noted before (after) the precipitation. Figures 2a,b show an example of a Mixed case. The high Z_{DR} values around and just within the CABS ring (along with the lower ρ_{HV} values) suggest biota contamination. More range gates are accumulated in higher class intervals away from the near-0 peak, resulting in reduced kurtosis. Most Mixed cases in this study consisted of predominately CABS returns with a few scans of contamination (e.g., light precipitation at the edge of the range domain); other Mixed cases are completely mixed for the entire time.

Cases were classified as Precip when precipitation returns covered the area or were much stronger than any visual CABS. Note in Figs. 2c,d how the main areas of concern are the fringes of precipitation that can pass the base data filters and become part of the statistical distribution. While many thresholds of dual-polarization variables and Z were tested individually and in combination to reduce precipitation contamination and to retain the most CABS cases, analysis revealed exemplary results solely with a 90th percentile of Z (Z90th) test. The Z values within the range and elevation angle limits were tabulated in a histogram with a class interval of 0.5 dBZ (the precision of the data) and with histogram limits of −32 and 40 dBZ. The class interval where 90% of the distribution falls below it is the location of the 90th percentile. Because CABS is characterized by low reflectivity returns ($Z < 10$ dBZ), a high Z90th would indicate precipitation contamination.

A scatterplot of Z90th for each of the cases shows a notable distinction between the CABS and Precip cases—a majority of the CABS cases fall below a line near −3.0 dBZ (Fig. 3). Moving the threshold from −2.0 to −3.0 dBZ results in a 1% loss of CABS cases and a 3% loss of Precip cases, while moving from −3.0 to −4.0 dBZ results in a 5% loss of CABS cases and only a 2% loss of Precip cases (Fig. 4). To balance the gains and losses of CABS and Precip, the value of Z90th $\leq$ −3.0 dBZ is sufficient as a filter for precipitation contamination.

Z90th is not expected to be an effective filter for None cases due to the sparse returns, so it is unsurprising that the percentage of None cases passing this filter are high. Filtering out Precip and Mixed cases was expected to be challenging—previous studies showed that CABS can be detected near, and possibly intensify from, light rain (Cohn et al. 1995; Knight and Miller 1998). Further investigations should be performed to assess Bragg scatter returns in said environments compared to CABS if used for Z_{DR} bias assessment.

g. *Algorithm summary*

An automated algorithm can be used to isolate CABS information from radar data. Because CABS is caused by randomly orientated turbulence, the intrinsic Z_{DR} is 0 dB and could be useful for determining whether a radar has a Z_{DR} bias. Our study uses the following steps to estimate the Z_{DR} bias from CABS returns:

1) Use spatial and temporal limits to mitigate contamination from clutter, some precipitation; focus on common CABS heights

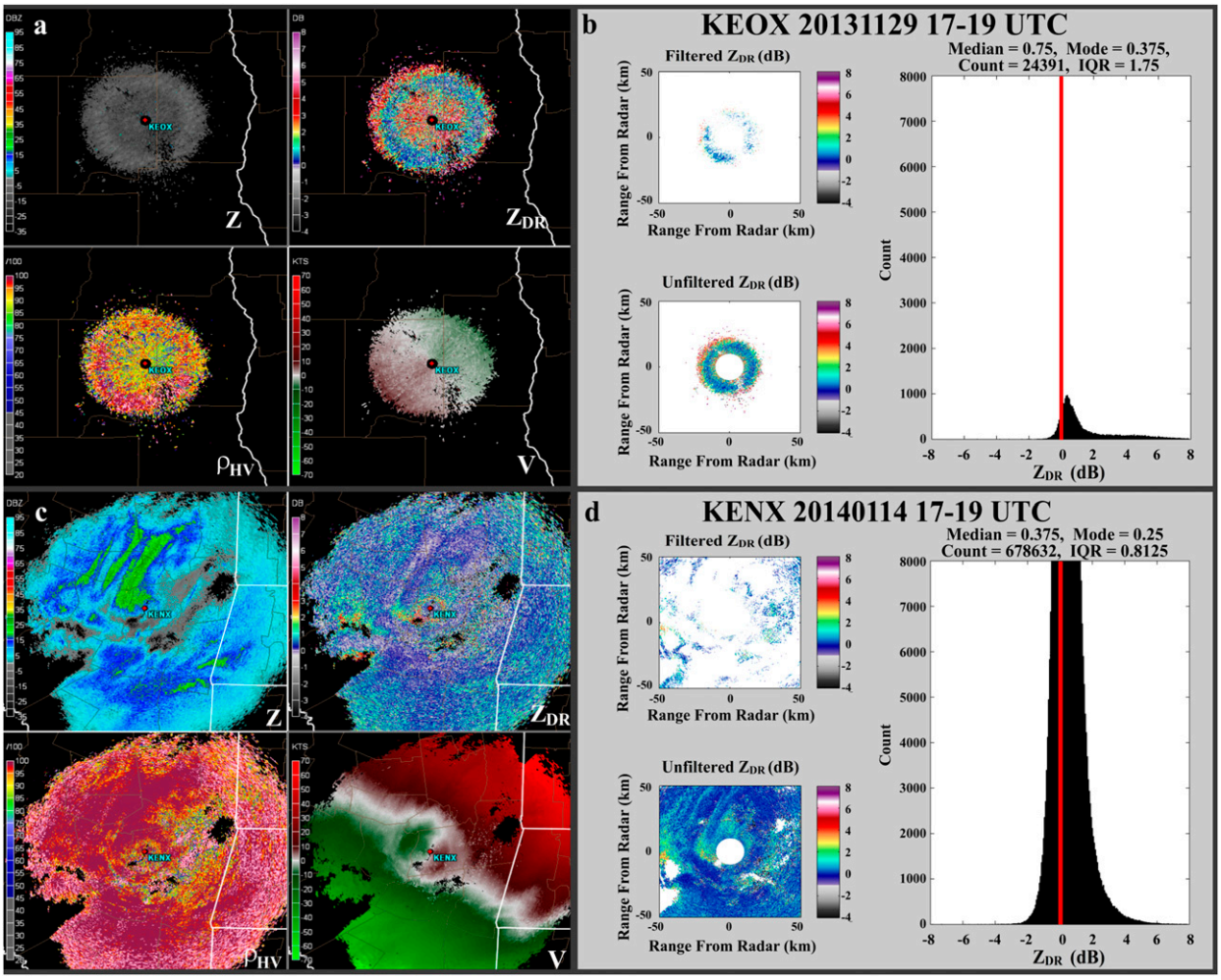

FIG. 2. (a),(b) Mixed case example with CABS and biota from Fort Rucker, AL (KEOX), on 29 Nov 2013 with the same layout as in Fig. 1. Radar data shown are from the 2.4° elevation angle at 1850 UTC; max range shown is ~50 km. Many biota returns have higher Z_{DR} than CABS, resulting in a thicker tail to the right and lower kurtosis. This case would not count as a valid CABS case due to the IQR filter. (c),(d) Precip example from Albany, NY (KENX), on 14 Jan 2014. Radar data shown are from the 3.5° elevation angle at 1858 UTC; max range is ~90 km. As CABS generally has less than 8000 range gates in any single category, the exceedance of this in the histogram is one indicator of the precipitation contamination passing the base data filters.

(i) Use only volume scans between 1700 and 1900 UTC
(ii) Use only volume scans in VCPs 21 and 32
(iii) Use only cuts (individual elevation scans) from 2.5° to 4.5°
(iv) Look only at range gates between 10 and 80 km

2) Collect all Z data within these spatial and temporal limits into a histogram
3) Collect all Z_{DR} data that pass the base data filters of Eq. (1) within the spatial and temporal limits into a histogram
4) Assess statistical validity and potential contamination of the Z_{DR} histogram
   (i) Total range gate count $\geq$ 10 000 range gates
   (ii) IQR $<$ 0.9 dB
5) Assess precipitation contamination using the Z histogram
   (i) Z90th ≤ -3.0 dBZ
6) If all of the previous conditions are satisfied, then use the mode of the Z_{DR} histogram as an estimate of Z_{DR} bias. Sites with nonzero decibel modes could suggest that a Z_{DR} bias exists for a given radar site.

3. Algorithm testing

Two techniques were employed to assess the algorithm output: visual confirmation and comparisons to sounding parameters. Visual confirmation entails looking at the radar fields using a display tool such as GR2Analyst (Gibson Ridge Software, LLC) and labeling the entire

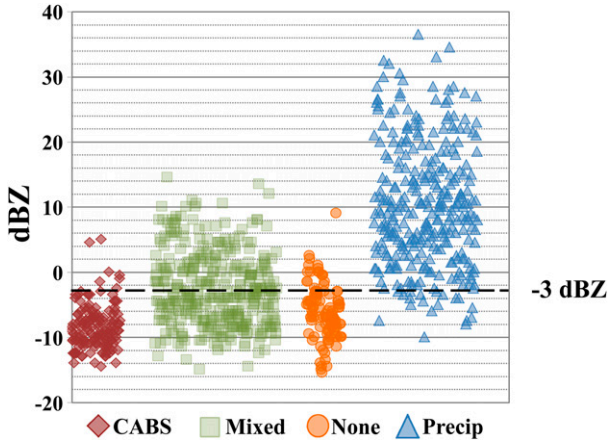

FIG. 3. Distribution of Z90th values for each case used for the precipitation filter study as per each visually assessed category described in section 2e. Cases are plotted per category along the x axis. The dashed black line (marking $-3.0\,\mathrm{dB}Z$) reveals that a majority of the CABS cases fall below this threshold, while a majority of Precip cases fall above this threshold.

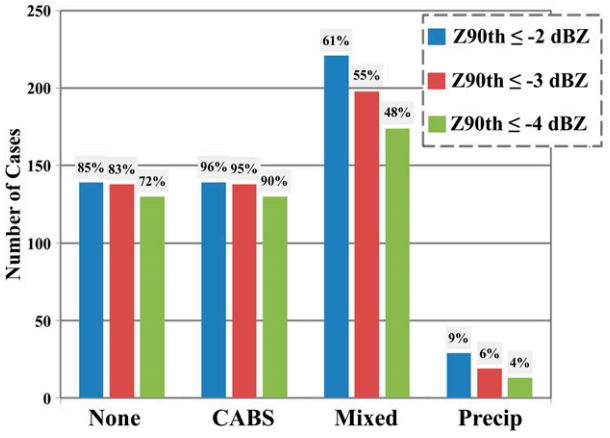

FIG. 4. Number and percentage of cases that pass with certain Z90th thresholds applied. Bar height represents the number of cases that pass per category, and the percentage of the category that pass is displayed above each bar.

case as falling in a certain category. This method assumes the authors have expertise in distinguishing CABS from other radar returns similar to the example in Fig. 1. In particular, a distinct ringlike feature with lower, more uniform Z_{DR} and higher ρ_{HV} is suggestive of CABS. Some stratus can appear as rings, and the automated routine would have a difficult time distinguishing this from CABS; yet the Z_{DR} characteristics of these features could still be useful for determining Z_{DR} bias. Precipitation often is characterized by higher Z and forms in more patchlike groups than rings. Biota has lower ρ_{HV} and Z_{DR} away from 0 (generally very high or very low) though it can often appear as rings.

For a second technique, parameters from soundings can be used to assess refractivity variations that are closely related to CABS. Information about moisture, temperature, and shear spanning different heights can be used to calculate parameters such as a relative humidity slope, the refractivity gradient, and the gradient Richardson number. We hypothesized that sounding tests should identify layers conducive to producing turbulence—a necessity for generating CABS. Therefore, radar-identified CABS should correlate with these sounding layers a majority of the time.

a. Results from the visual dataset

Using the 919 cases mentioned in section 2f, experts classified 145 cases as CABS, 361 cases as Mixed, 308 cases as Precip, and 105 cases as None. Cases were processed through the complete algorithm to check how many cases from each category would pass and give a Z_{DR} bias estimate (Fig. 5). A majority (81%) of the CABS cases remain while considerably reducing the Mixed, Precip, and None cases (26%, 4%, and 6% remain, respectively). Though almost 20% of CABS cases are excluded, nearly all of the None and Precip cases are successfully ignored. Excluding 20% of CABS cases is acceptable in order to omit the majority of contaminated cases. As previously mentioned, some light precipitation may still pass the filters, but small drops with near 0-dB Z_{DR} should not impact the estimate from a Z_{DR} bias perspective.

About half (52 of 93) of the Mixed cases that passed contained CABS throughout the time domain, so the contribution from contaminants could be small enough

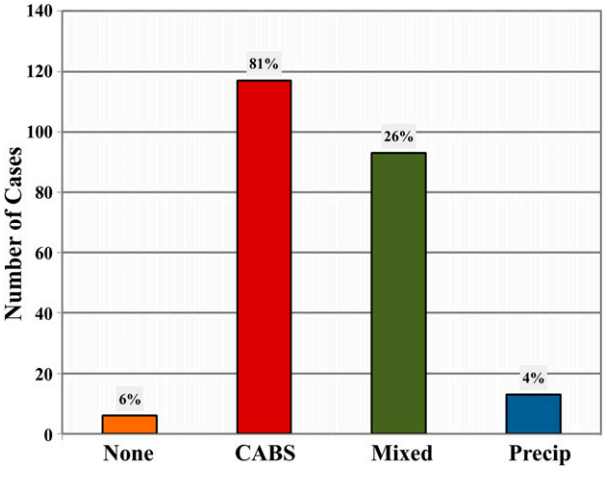

FIG. 5. Number and percentage of visually analyzed cases that pass the CABS routine, i.e., that pass the base data, statistical, and precipitation filters. Bar height represents the number of cases per category that pass, and the percentage of the category that pass is displayed above each bar.

to not affect the Z_{DR} bias estimate. Many cases had only one volume scan with potential contamination, which by our strict rules caused it to be classified as a Mixed case. Three of the five None cases had CABS visually too close to the radar (less than 10 km) but received enough returns around 10 km to pass the range gate count filter. Such cases could potentially be useful as Z_{DR} bias estimates from CABS. The remaining two None cases that passed had notable biota and ground clutter range gates that managed to pass through the multiple stages of filtering.

Visual confirmation results suggest this algorithm can successfully detect and filter CABS from other types of radar returns a majority of the time. Cases that passed with contamination were seen to have CABS throughout the time domain, and the impact of such cases on Z_{DR} bias estimation should be addressed in future studies. While visual radar analysis by experts can be used to assess the existence of CABS from a radar, thermodynamic profiles from sounding data could confirm the existence of a potential CABS layer.

b. Sounding confirmation

The authors examined sounding data to evaluate the presence of a potential CABS layer compared to the radar data. Only radars within 100 km of a radiosonde station were selected to facilitate matching atmospheric characteristics; there were 95 paired radar–sounding sites in total. Sparsity of vertical resolution, site elevation differences, and horizontal distances could prevent matching of characteristics from the sounding and radar data in some cases, but general tests were explored as a potentially useful verification metric. Archived 0000 UTC sounding data from the University of Wyoming (2014) were gathered and linearly interpolated to provide a vertical resolution of 50 m for October 2013–September 2014 data. A case consists of radar data from 0000 to 0200 UTC processed with the CABS algorithm paired with the 0000 UTC sounding data.[7] Relative humidity slope, refractivity gradient, and gradient Richardson number tests were selected to detect areas that may be conducive to producing CABS.

To ensure comparable datasets, radar data operating in an allowed VCP and available sounding data were required. From Table 1a, over a third of the site–date combination pairs did not use an allowed VCP. Cases with missing radar data (errors with the internal feed or the radar was down for maintenance) or missing sounding data were excluded from the comparison and decreased the dataset further. Cases with short sounding traces (less than 5000 m AGL) were also ignored because of the lack of data for our test window. These minimum requirements yielded a set of 15 463 cases (Table 1b).

TABLE 1. Number and percentage of cases from the radar and sounding comparison set within various validation groups.

(i)	No. of cases	Total (%)
Total radar–sounding cases	34 675	
Wrong VCP	13 356	39
Radar data not available	671	2
No sounding	5185	15
(ii)	**No. of cases**	**Comparable (%)**
Comparable set	15 463	
Pass range gate test	11 252	73
Pass IQR test	4822	31
Pass Z90th test	4900	32
Pass RHS test	6410	41
Pass RG test	4695	30
Pass R_i test	6962	45
(iii)	**No. of cases**	**Valid (%)**
Valid set	929	
Valid with passing RHS	526	57
Valid with passing RG	473	51
Valid with passing R_i	503	54
Valid with RHS or RG or R_i	795	86
Valid without RHS or RG or R_i	134	14

1) SOUNDING PARAMETERS

Davison et al. (2013a,b) showed several instances of how Bragg scattering layers (not necessarily clear air) in a marine environment relate to thermodynamic profile characteristics. In particular, they state there are often a relative humidity maximum at the base of a Bragg scattering layer and a relative humidity minimum at the top of the layer. Testing for a negative slope in relative humidity could indicate a layer of Bragg scattering. Relative humidity slope (RHS) is calculated as follows:

$$\mathrm{RHS} = \frac{\mathrm{RH}_{\max} - \mathrm{RH}_{\min}}{z_{\mathrm{RHmax}} - z_{\mathrm{RHmin}}}, \tag{2}$$

where z is the height (m) and the maximum and minimum values are determined from a given layer.

Davison et al. (2013a) also demonstrated a close relationship between vertical relative humidity and refractivity gradients. The vertical gradient of refractivity is dependent on vertical gradients of temperature, dewpoint, and pressure. The index of refraction

[7] The 0000–0200 UTC dataset was chosen instead of 2300–0100 UTC to avoid crossing dates in order to streamline processing.

n is related to refractivity N as (Bean and Dutton 1966) follows:

$$N = (n-1)\times 10^6. \tag{3}$$

The refractivity gradient (RG) is related to temperature, moisture, and pressure by [Eq. (3) in Davison et al. 2013a]

$$\frac{\Delta N}{\Delta z} = 77.6\frac{1}{T}\frac{\Delta p}{\Delta z} - \left(77p - 5.6Se_s + 7.5\times 10^5\frac{Se_s}{T}\right)\frac{1}{T^2}\frac{\Delta T}{\Delta z} + \left(-5.6 + 3.75\times 10^5\frac{1}{T}\right)\frac{S}{T}\frac{\Delta e_s}{\Delta z} + \left(-5.6 + 3.75\times 10^5\frac{1}{T}\right)\frac{e_s}{T}\frac{\Delta S}{\Delta z}, \tag{4}$$

where T is the temperature (K), z is height (m), p is the pressure (mb), S is the saturation ratio, and e_s is the saturation vapor pressure (mb). The RHS and RG test are likely to have a strong correlation to CABS because CABS has more dependence on moisture and temperature than pressure. Results from Ottersten (1969) confirm that pressure gradients are not as important in CABS development.

A majority of CABS layers correspond to turbulent layers in the atmosphere. Thus, it is expected that most CABS layers correspond with a certain gradient Richardson number value (R_i), where R_i is calculated as

$$R_i = \frac{N_{\mathrm{BV}}^2}{\dfrac{\Delta u^2}{\Delta z} - \dfrac{\Delta v^2}{\Delta z}}, \tag{5}$$

where u and v are the horizontal and vertical wind speeds ($\mathrm{m\,s^{-1}}$), respectively; z is vertical height (m); and N_{BV} is the Brunt–Väisälä frequency, defined as

$$N_{\mathrm{BV}} = \sqrt{\frac{g}{\theta_v}\frac{\Delta\theta_v}{\Delta z}}, \tag{6}$$

where θ_v is the virtual potential temperature (K) and g is gravity ($\mathrm{m\,s^{-2}}$). Balsley et al. (2008) showed that R_i intensity varies with the depth used in the calculation, yet they also demonstrated that 50 m is a reasonable scale for turbulence estimations. For this study, R_i values were ignored below 500 m AGL because the range and elevation angle restrictions on the radar typically start at and are above this height.

2) Parameter thresholds

Various threshold values for the tests were assessed within a ±250-m window around the modal height of detected radar range gates. Only sounding data below 5000 m (AGL) were considered for each threshold test. The mode of radar range gate heights, RHS, RG, and R_i values were all adjusted and related to above mean sea level (MSL) measurements for the ±250-m window comparison. Cases of radar-indicated CABS from October 2013 were used to find testable thresholds with the consideration that thresholds may vary regionally and seasonally (Fig. 6).

Relative humidity was shown to decrease by at least 10% over 500 m in Davison et al. (2013a,b), yet their cases are exclusively maritime. In more arid regions (such as Arizona), some of the October cases suggest a relative humidity decrease of 7.5% over 500 m corresponds well with CABS. The lower threshold, equating to RHS $\leq -1.5\times 10^{-4}\,\mathrm{m^{-1}}$, served as the RHS threshold in this study to better capture various climate regimes. Generally, the RHS can be much steeper as suggested by Fig. 6a, where the median value is $-5.1\times 10^{-4}\,\mathrm{m^{-1}}$. For RG and R_i, CABS is generally denoted by a minimum in the parameters. Typical RG minimum values associated with CABS are $\leq -0.070\,\mathrm{m^{-1}}$, and R_i minimum values ≤ 0.20 were seen to correlate with CABS cases for the October subset (which are close to the medians in Figs. 6b,c). Though R_i values below the critical Richardson number of 0.25 denote regions conducive to generating turbulence (Thorpe 1969; Scotti and Corcos 1969), not all turbulent layers are favorable for CABS. Thus, an R_i estimate alone is not sufficient to validate a CABS layer.

3) Sounding results

The sounding results were compared to potential radar-detected CABS in two different ways. In the first instance, the CABS algorithm filters did not have to be met (labeled "Comparable" in Table 1b); the only requirements were that both radar data and sounding data were available (and the radar data had to be in an allowed VCP). In the second instance, the test for CABS had to pass all radar algorithm filters (labeled "Valid" in Table 1c). Note that the Valid set is a subset of the Comparable set. Cases in the Comparable set were pared down by the algorithm filters to retain cases containing radar-estimated CABS with valid sounding data. Many cases failed to pass the Z90th and IQR tests, which is expected because many days likely contain precipitation and biota contamination (i.e., days in this sample set were not preselected as CABS cases). A majority of the cases (73%) passed the range gate count filter but only 31% and 32% of cases passed the Z90th and IQR filters, respectively. With contamination possibly included, the RHS test suggested a conducive layer within the ±250-m window 41% of the time, the RG test suggests a conducive layer 30% of the time, and the R_i test suggests a conducive layer 45% of the time in the Comparable set. Several cases pass the sounding tests

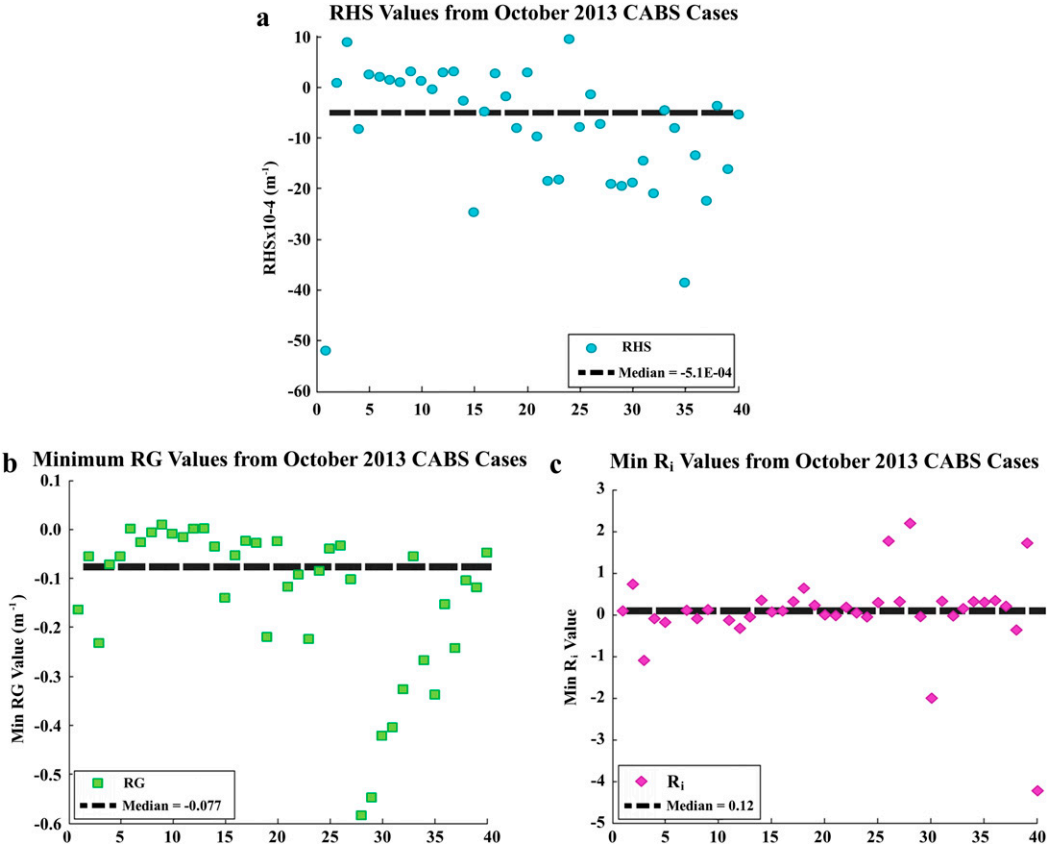

FIG. 6. (a) RHS, (b) minimum RG, and (c) minimum R_i values for 0000–0200 UTC Oct 2013 cases that pass the CABS algorithm. The dashed line in each plot represents the median value. Out of all radar–sounding pairs, only ~40 cases passed. These cases, plotted in no specific radar/date order along the x axis, were used to determine a relative threshold for the RHS, RG, and R_i tests.

but do not pass the CABS filters. For example, 41% of cases pass the RHS test but only 31% of cases pass the IQR test. Contamination that can skew the appropriate modal height window to look for RHS, RG, and R_i could contribute to false alarms in the Comparable set.

Cases that pass the base data, statistical, and precipitation filters were denoted CABS and were considered the Valid set (Table 1c). Sounding tests (RHS, RG, and R_i) were estimated for each ''Valid CABS'' case in a nonexclusive manner; that is, the RHS, RG, and R_i tests could pass individually or together on the same case. Altogether, sounding tests relate to radar-indicated CABS cases 86% of the time. Each test relates to a CABS case around 50% of the time, and much less when considered exclusively. For the nonmatching 14%, the threshold values may be falling just outside of the ±250-m window or be just beyond the thresholds chosen for each test. Conversely, the radar-reported CABS could include contamination and the sounding tests are correctly not identifying a layer.

c. *Sounding case studies*

To further assess the commonality and disparity between the radar and sounding tests, three case studies will be presented here. An example of a CABS case and the associated sounding parameter profile from Fort Campbell, Kentucky (KHPX), on 5 April 2014 is shown in Fig. 7. This case passes all of the filters in the algorithm and would be considered a Valid case. The CABS ring is very distinct and separated from the clutter/biota immediately surrounding the radar (Fig. 7a). Both the CABS and clutter/biota returns appear as peaks in the radar range gate profile histogram (Fig. 7b), and the CABS layer peaks around 2000 m (MSL). The dashed green lines represent the ±250-m window around this radar range gate height mode. A sharp minimum layer is present in both the RG and R_i fields within this window along with a notable decrease in RH across the layer. The black dotted lines in the RG and R_i fields denote the thresholds for passing used in this study. There is only one RG layer in the profile, and it

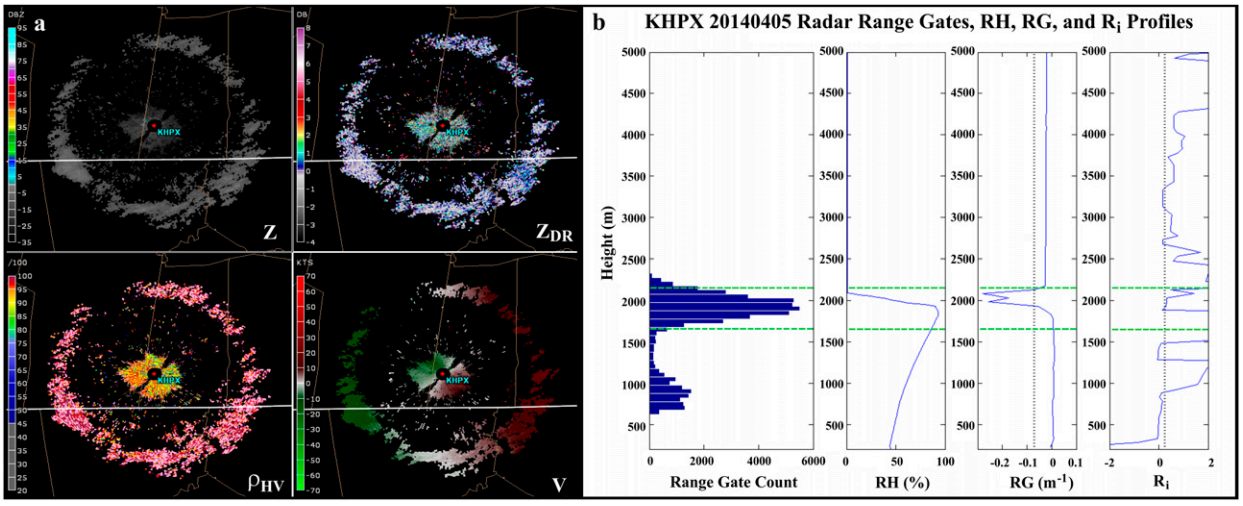

FIG. 7. (a) Radar example of a CABS case from Fort Campbell, KY (KHPX), on 5 Apr 2014 from the 3.5° elevation angle at 0008 UTC. Maximum range shown in the radar image is ~37 km. (b) The associated profile with height of the radar range gates, RHS, RG, and R_i. The black vertical dotted lines represent the test threshold for the sounding parameters, and the green dashed line represents the ±250-m window around the mode of radar range gate heights. Sounding data came from the Nashville, TN, 0000 UTC radiosonde (~97 km away from the radar site).

corresponds well with the potential CABS layer denoted by the radar data. Meanwhile, there are several instances of lower R_i. Notice the sharp change in R_i at the surface, which may be caused by actual near-surface conditions or could be an artifact of the calculation and interpolated sounding data. Recall that any values within the first 500 m (AGL) are ignored to help mitigate these effects. Though the RHS, RG, and R_i tests all match here, this cannot always be expected with CABS and/or the radar-estimated returns.

An example from King Salmon, Alaska (PAKC), on 26 July 2014 (Fig. 8) appears visually to be a distinct CABS layer (even if the ring is not complete due to the terrain/coastline). This case also passes all of the filters in the algorithm and would be considered Valid. Radar range gates from the CABS layer match in height with a notable negative slope in relative humidity and a minimum in RG, but they lack a minimum in R_i. Again, the manner of calculation, the interpolated data, or other atmospheric dynamic properties, such as a very stable layer in the large-scale sounding, may be contributing to this nonmatch in R_i.

Sometimes cases with contamination pass the RG and R_i tests. A case with biota and precipitation from Corpus

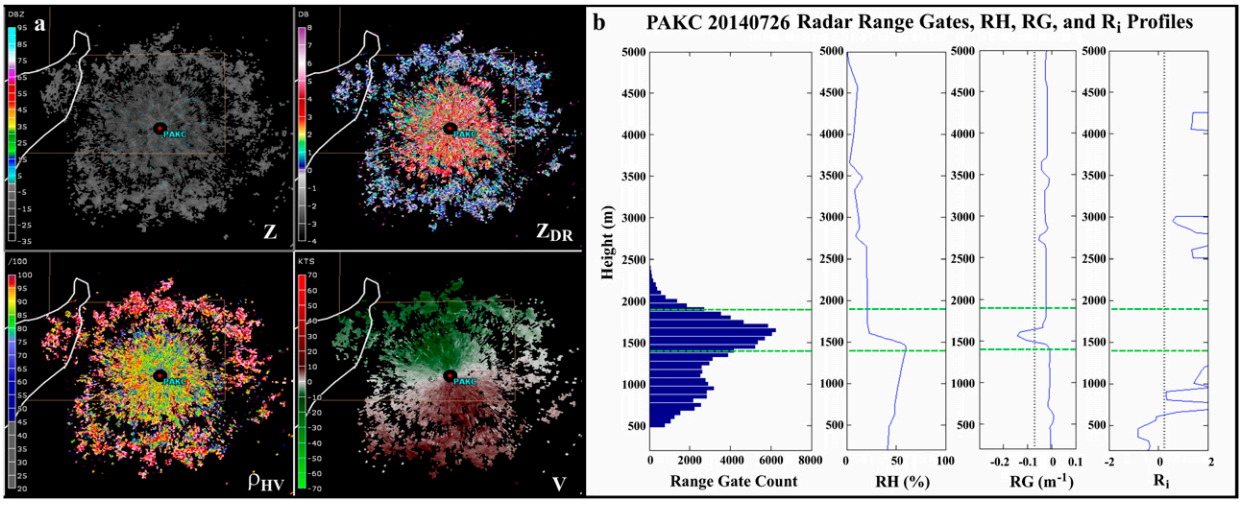

FIG. 8. Example of a CABS case that passes only the RHS and RG tests from King Salmon, AK (PAKC), on 26 Jul 2014, in the same layout as in Fig. 7. The radar image is from the 3.5° elevation angle at 0115 UTC; the maximum range shown is ~42 km. Sounding data came from the King Salmon 0000 UTC radiosonde (less than 1 km away from the radar site).

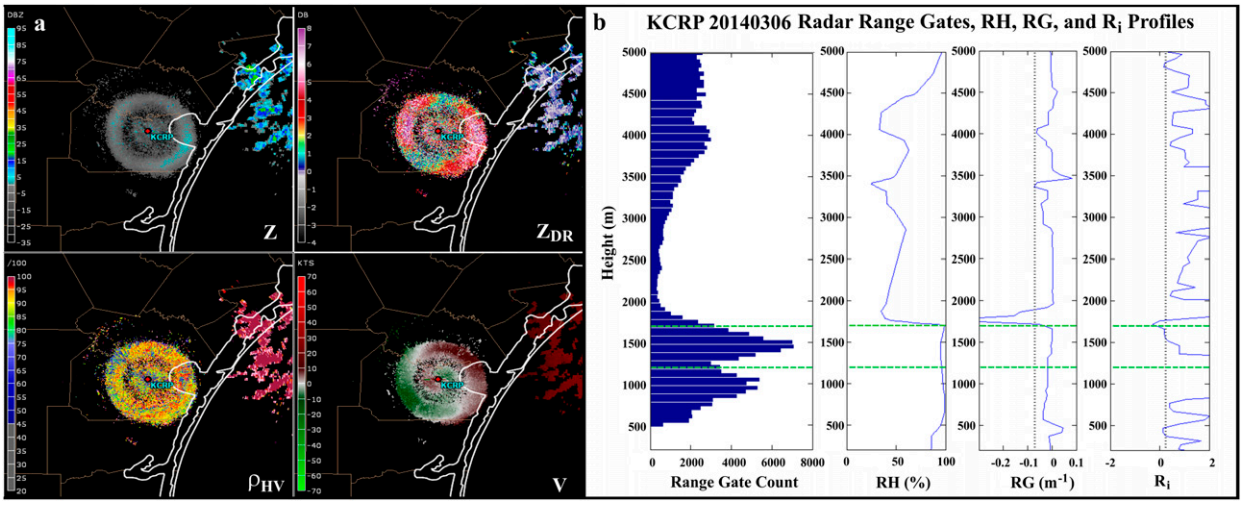

FIG. 9. Example of a CABS case saturated with biota and contaminated with separate precipitation returns (within the 10–80-km limit) from Corpus Christi, TX (KCRP), on 6 Mar 2014, in the same layout as in Fig. 7. The radar image is from the 3.5° elevation angle at 0119 UTC; the maximum range shown is ~83 km. Sounding data came from the Corpus Christi 0000 UTC radiosonde (less than 1 km away from the radar site).

Christi, Texas (KCRP), on 6 March 2014 (Fig. 9) shows passing R_i values and an RG minimum and RHS just outside of the window limit. Visually, the radar image shows noticeable biota contamination in a potential CABS layer due to the high Z_{DR} and lower ρ_{HV} values (yellows instead of magenta/pink). The smooth ρ_{HV} and higher Z values east of the radar denote the precipitation returns that contribute to the higher height returns in the histogram up to 5000 m (MSL). Even if the profile parameters suggest a potential CABS layer, this case would be unusable for Z_{DR} bias estimations due to the heavy contamination. The algorithm successfully captures this contamination, as the case failed to pass the IQR portion of the statistical filters and does not count as a Valid case.

4. Summary and discussion

Studies over the past several years have shown that layers of clear-air Bragg scatter can be observed by radars. Information about such layers, besides assisting with locating the height of maritime and continental boundary layers, can assess Z_{DR} bias for a given WSR-88D.[8] An algorithm was designed to assist with estimating Z_{DR} bias by using CABS returns.

Level II data from the WSR-88D network is a widely available resource that permits CABS studies across more regimes than the mostly coastal and plains studies. This study explored using these radar data and a priori knowledge of the characteristics of base data moments and dual-polarization fields to develop an algorithm to use CABS returns. Specific range, elevation angle, and VCP requirements were selected to help avoid contamination from ground clutter and certain types of precipitation. Data from CONUS and OCONUS radars were analyzed from October 2013 to September 2014 using a 1700–1900 UTC time window and, separately, a 0000–0200 UTC time window. It is noted that limited time windows may not be optimal for all sites because of the time of day selected, but the windows selected for this study generally contain adequate heating across a majority of the sites to find CABS.

A set of base data filters, described in Eq. (1), places Z_{DR} values from passing range gates into a histogram. Application of statistical filters on the 2-h accumulated histogram reduces contamination from biota and precipitation and ensures sufficient range gates for statistical analysis. A subset of 1700–1900 UTC data (October 2013–March 2014) was used to create an additional filter for precipitation contamination. Cases were visually separated into four categories: Bragg, Mixed, None, and Precip as described in section 2e. Results showed that using a 90th percentile of Z (Z90th) threshold of ≤ -3.0 dBZ effectively reduces Precip cases that pass the base data and statistical filters.

The subset data were also used for visual confirmation of the algorithm's output. With the inclusion of the base data, statistical, and precipitation filters, the majority of CABS cases (81%) are accurately confirmed, while only minimal cases of contamination remain (6% of None and 4% of Precip cases). About half of the passing Mixed cases contained mostly CABS throughout the 2-h time window, though only 26% of Mixed cases passed our strict criteria. As a few cases of contamination still

[8] While many S-band radars can detect CABS, some S-band radars do not have enough sensitivity to detect the weak signals.

pass through the current filter set, future studies should explore refining or creating new filters to improve CABS detection without contamination. Stricter filters could be used if pristine quality of estimates is needed, but increased strictness may severely limit the number of Z_{DR} bias estimates from CABS.

Additionally, the 0000–0200 UTC dataset was compared to 0000 UTC sounding parameters to calculate relative humidity slope, refractivity gradient, and gradient Richardson number values. Results in Table 1c show that the three sounding tests explored here match well with radar-indicated CABS. While the sounding tests suggest only layers conducive to CABS, confirmation of necessary atmospheric conditions supports the premise that the algorithm is successfully capturing CABS data.

The algorithm presented here is designed to work with operational WSR-88Ds (i.e., it does not require special scanning strategies or dwell times). The removal of VCP limits should be investigated to assess the potential for finding more Z_{DR} bias estimates from CABS from sites that rarely use the current requisite VCPs. While only a 2-h window study was performed, CABS can occur and last throughout multiple hours in a day. Though specific filters were used for this test, these thresholds are not defined with hard limits and could be adjusted for future studies. Information from this algorithm could be successfully implemented to help assess Z_{DR} bias [explored further in Part II (Richardson et al. 2017)] or for wide-scale assessment of boundary layer studies. CABS is an additional target of information readily available from the WSR-88D fleet.

Acknowledgments. The authors sincerely thank the Radar Operations Center Data Quality Committee, Dr. James Correia Jr., David Cleaver, Nicholas Cooper, and their dedicated and supportive colleagues for their assistance with this study and document. This material is based upon work supported by the National Science Foundation under Grant No. AGS-1062932. We also appreciate the comments from the anonymous reviewers, which helped to clarify and strengthen this document.

REFERENCES

Atlas, D., 1959: Meteorological "angel" echoes. *J. Meteor.*, **16**, 6–11, doi:10.1175/1520-0469(1959)016<0006:ME>2.0.CO;2.

Balsley, B. B., G. Svensson, and M. Tjernström, 2008: On the scale-dependence of the gradient Richardson number in the residual layer. *Bound.-Layer Meteor.*, **127**, 57–72, doi:10.1007/s10546-007-9251-0.

Bean, B. R., and E. J. Dutton, 1966: *Radio Meteorology. NBS Monogr.*, No. 92, U.S. Government Printing Office, 435 pp., doi:10.5962/bhl.title.38144.

Cohn, S. A., 1994: Investigations of the wavelength dependence of radar backscatter from atmospheric turbulence. *J. Atmos. Oceanic Technol.*, **11**, 225–238, doi:10.1175/1520-0426(1994)011<0225:IOTWDO>2.0.CO;2.

——, R. R. Rogers, S. Jascourt, W. L. Ecklund, D. A. Carter, and J. S. Wilson, 1995: Interactions between clear-air reflective layers and rain observed with a boundary layer wind profiler. *Radio Sci.*, **30**, 323–341, doi:10.1029/94RS03168.

Cowley, J. M., 1995: *Diffraction Physics.* 3rd ed. North-Holland, 481 pp.

Crum, T. D., R. L. Alberty, and D. W. Burgess, 1993: Recording, archiving, and using WSR-88D data. *Bull. Amer. Meteor. Soc.*, **74**, 645–653, doi:10.1175/1520-0477(1993)074<0645:RAAUWD>2.0.CO;2.

Cunningham, J. G., W. D. Zittel, R. R. Lee, and R. L. Ice, 2013: Methods for identifying systematic differential reflectivity (Zdr) biases on the operational WSR-88D network. *36th Conf. on Radar Meteorology*, Breckenridge, CO, Amer. Meteor. Soc., 9B.5. [Available online at https://ams.confex.com/ams/36Radar/webprogram/Paper228792.html.]

Davison, J. L., R. M. Rauber, and L. Di Girolamo, 2013a: A revised conceptual model of the tropical marine boundary layer. Part II: Detecting relative humidity layers using Bragg scattering from S-band radar. *J. Atmos. Sci.*, **70**, 3025–3046, doi:10.1175/JAS-D-12-0322.1.

——, ——, ——, and M. A. LeMone, 2013b: A revised conceptual model of the tropical marine boundary layer. Part III: Bragg scattering layer statistical properties. *J. Atmos. Sci.*, **70**, 3047–3062, doi:10.1175/JAS-D-12-0323.1.

Doviak, R. J., and D. S. Zrnić, 2006: *Doppler Radar and Weather Observations.* 2nd ed. Dover Publications, 562 pp.

Gage, K. S., C. R. Williams, W. L. Ecklund, and P. E. Johnston, 1999: Use of two profilers during MCTEX for unambiguous identification of Bragg scattering and Rayleigh scattering. *J. Atmos. Sci.*, **56**, 3679–3691, doi:10.1175/1520-0469(1999)056<3679:UOTPDM>2.0.CO;2.

Hardy, K. R., and I. Katz, 1969: Probing the clear atmosphere with high power, high resolution radars. *Proc. IEEE*, **57**, 468–480, doi:10.1109/PROC.1969.7001.

——, and H. Ottersten, 1969: Radar investigations of convective patterns in the clear atmosphere. *J. Atmos. Sci.*, **26**, 666–672, doi:10.1175/1520-0469(1969)26<666:RIOCPI>2.0.CO;2.

Heinselman, P. L., P. L. Spencer, K. L. Elmore, D. J. Stensrud, R. M. Hluchan, and P. C. Burke, 2009: Radar reflectivity–based estimates of mixed layer depth. *J. Atmos. Oceanic Technol.*, **26**, 229–239, doi:10.1175/2008JTECHA1091.1.

Hoban, N. P., J. G. Cunningham, and W. D. Zittel, 2014: Estimating systematic WSR-88D differential reflectivity (ZDR) biases using Bragg scattering. *30th Conf. on Environmental Information Processing Technologies*, Atlanta, GA, Amer. Meteor. Soc., 2. [Available online at http://ams.confex.com/ams/94Annual/webprogram/Manuscript/Paper237404/Final_Extend_Abstract_AMS_Feb2014.pdf.]

Ivić, I. R., 2014: On the use of a radial-based noise power estimation technique to improve estimates of the correlation coefficient on dual-polarization weather radars. *J. Atmos. Oceanic Technol.*, **31**, 1867–1880, doi:10.1175/JTECH-D-14-00052.1.

——, C. Curtis, and S. M. Torres, 2013: Radial-based noise power estimation for weather radars. *J. Atmos. Oceanic Technol.*, **30**, 2737–2753, doi:10.1175/JTECH-D-13-00008.1.

——, J. C. Krause, O. E. Boydstun, A. E. Daniel, A. D. Free, and W. D. Zittel, 2014: Effects of radial-based noise power estimation on spectral moment estimates. *J. Atmos. Oceanic Technol.*, **31**, 2671–2691, doi:10.1175/JTECH-D-14-00048.1.

Kaimal, J. C., and Coauthors, 1982: Estimating the depth of the daytime convective boundary layer. *J. Appl. Meteor.*, **21**, 1123–1129, doi:10.1175/1520-0450(1982)021<1123:ETDOTD>2.0.CO;2.

Knight, C. A., and L. J. Miller, 1993: First radar echoes from cumulus clouds. *Bull. Amer. Meteor. Soc.*, **74**, 179–188, doi:10.1175/1520-0477(1993)074<0179:FREFCC>2.0.CO;2.

——, and ——, 1998: Early radar echoes from small warm cumulus: Bragg and hydrometeor scattering. *J. Atmos. Sci.*, **55**, 2974–2992, doi:10.1175/1520-0469(1998)055<2974:EREFSW>2.0.CO;2.

Melnikov, V. M., and D. S. Zrnić, 2007: Autocorrelation and cross-correlation estimators of polarimetric variables. *J. Atmos. Oceanic Technol.*, **24**, 1337–1350, doi:10.1175/JTECH2054.1.

——, R. J. Doviak, D. S. Zrnić, and D. J. Stensrud, 2011: Mapping Bragg scatter with a polarimetric WSR-88D. *J. Atmos. Oceanic Technol.*, **28**, 1273–1285, doi:10.1175/JTECH-D-10-05048.1.

——, ——, ——, and ——, 2013a: Structures of Bragg scatter observed with the polarimetric WSR-88D. *J. Atmos. Oceanic Technol.*, **30**, 1253–1258, doi:10.1175/JTECH-D-12-00210.1.

——, D. Zrnić, M. Schmidt, and R. Murnan, 2013b: Z_{DR} calibration issues in the WDR-88Ds: Report on 2013-MOU. NSSL Rep., NOAA, 54 pp. [Available online at http://www.nssl.noaa.gov/publications/wsr88d_reports/WSR88D_ZDRcalib_Report_2013.pdf.]

Ottersten, H., 1969: Atmospheric structure and radar backscattering in clear air. *Radio Sci.*, **4**, 1179–1193, doi:10.1029/RS004i012p01179.

Richardson, L. M., W. D. Zittel, R. R. Lee, V. M. Melnikov, R. L. Ice, and J. G. Cunningham, 2017: Bragg scatter detection by the WSR-88D. Part II: Assessment of Z_{DR} bias estimation. *J. Atmos. Oceanic Technol.*, **34**, 479–493, doi:10.1175/JTECH-D-16-0031.1.

Scotti, R. S., and G. M. Corcos, 1969: Measurements on the growth of small disturbances in a stratified shear layer. *Radio Sci.*, **4**, 1309–1313, doi:10.1029/RS004i012p01309.

Stensrud, D. J., 2007: Planetary boundary layer and turbulence parameterizations. *Parameterization Schemes: Keys to Understanding Numerical Weather Prediction Models*. Cambridge University Press, 138–184.

Thorpe, S. A., 1969: Experiments on the stability of stratified shear flows. *Radio Sci.*, **4**, 1327–1331, doi:10.1029/RS004i012p01327.

University of Wyoming, 2014: Atmospheric soundings. Department of Atmospheric Science, University of Wyoming. Subset used: October 2013–September 2014, accessed 12 October 2014. [Available online at http://weather.uwyo.edu/upperair/sounding.html.]

vanZanten, M. C., P. G. Duynkerke, and J. W. M. Cuijpers, 1999: Entrainment parameterization in convective boundary layers. *J. Atmos. Sci.*, **56**, 813–828, doi:10.1175/1520-0469(1999)056<0813:EPICBL>2.0.CO;2.

Wilks, D. S., 2006: *Statistical Methods in the Atmospheric Sciences*. 2nd ed. International Geophysics Series, Vol. 91, Academic Press, 627 pp.

WSR-88D ROC, 2008: WSR-88D system specification revision H. NWS Radar Operations Center Rep. ROC/2810000H/0WY55, 160 pp.

Zittel, W. D., J. G. Cunningham, R. R. Lee, L. M. Richardson, R. L. Ice, and V. Melnikov, 2014: Use of hydrometeors, Bragg scatter, and sun spikes to determine system Z_{DR} biases in the WSR-88D fleet. Extended Abstracts, *Eighth European Conf. on Radar in Meteorology and Hydrology (ERAD 2014)*, Garmisch-Partenkirchen, Germany, DWD and DLR, DAC.P12. [Available online at https://www.roc.noaa.gov/WSR88D/PublicDocs/Publications/132_Zittel.pdf.]